

# Heterogeneous Solid-Electrolyte Interphase in Graphite Electrodes Assessed by 4D-Resolved Computational Simulations

Mehdi Chouchane,<sup>[a, b]</sup> Oier Arcelus,<sup>[a, b]</sup> and Alejandro A. Franco<sup>\*[a, b, c, d]</sup>

Graphite is one of the most used active materials in lithium-ion battery negative electrodes thanks to its high specific capacity and low equilibrium potential. For over 40 years, one of the most discussed issues with this material revolves around the complex formation mechanism of the solid-electrolyte interphase (SEI), which acts as a protective layer against electrolyte decomposition but causes capacity losses. Due to the difficulties to experimentally observe the SEI (air sensibility, low contrast and nanometric size), its impact on the performance of graphite-based porous electrodes has never been spatially assessed in regards of the three-dimensional features of the electrodes. We report here a new 4D (3D + time) resolved computational model which gives insights about the SEI heterogeneity within such porous electrodes. The model is applied to different graphite morphologies and is able to assess the electrode mesostructure impact on the SEI formation and the impact of the latter on the electrodes' electrochemical performance. This work paves the way towards a powerful tool to assist in the interpretation of SEI characterization experiments.

Nowadays graphite is one of the most used negative electrode materials in lithium-ion batteries (LIBs).<sup>[1]</sup> Its ability to intercalate Li has been known since 1975<sup>[2]</sup> but all endeavors to achieve reversible intercalation were unsuccessful because of graphite exfoliation and instabilities in the electrolyte.<sup>[3,4]</sup> The first reported reversible cycle with graphite using a polymer electrolyte was done in 1983 by Yazami and Touzain.<sup>[5]</sup> Later, in

1990,<sup>[6]</sup> Dahn *et al.* highlighted the possible use of ethylene carbonate (EC) as a liquid electrolyte in order to form a passivating layer around the graphite, now known as solid electrolyte interphase (SEI). Further investigation on the electrolyte formulation led Guyomard and Tarascon to identify, in 1993, a dimethyl carbonate (DMC) and EC mixture as an excellent candidate to improve the cyclability of graphite-based electrodes.<sup>[7]</sup>

Despite tremendous efforts to better understand and control the SEI formation its mechanism has been subject to debate for 40 years.<sup>[8]</sup> For instance, it is disputed whether the electrolyte reduction occurs at the graphite/electrolyte interface, or at the SEI/electrolyte interface, with the electrons transferring from the graphite to the SEI by tunneling effect.<sup>[9]</sup> Numerous first principles and mathematical models have been reported to shed light on the SEI growth process,<sup>[9–13]</sup> but still at a very local scale (electrode/electrolyte interface) or by oversimplifying the actual porous electrode mesostructure, described either through effective parameters (e.g. porosity and tortuosity factor like in the so-called pseudo-2D model), either through a 1D representation of the system. It is noteworthy that these type of models have been also used in the battery context to simulate lithium plating.<sup>[14]</sup>

Among the latter approaches, we can refer to the work of Pinson and Bazant<sup>[15]</sup> in which the rate of growth of the SEI,  $i_{\text{SEI}}$ , was described with a Butler-Volmer law in the same manner as the Li intercalation rate [Eq. (1)]

$$i_{\text{SEI}} = k_{\text{SEI}} \sqrt{c_e c_s} \left( e^{\frac{F\eta_{\text{SEI}}}{2RT}} - e^{-\frac{F\eta_{\text{SEI}}}{2RT}} \right) \quad (1)$$

where  $k_{\text{SEI}}$  is a kinetic constant;  $c_e$  and  $c_s$  are the  $\text{Li}^+$  concentration and Li concentration at the SEI interface, respectively, and  $\eta_{\text{SEI}}$  is the overpotential taking into account the resistance due to the SEI. Following a similar approach, Kolzenberg *et al.*<sup>[16]</sup> defined the rate of growth of the SEI as directly proportional to the intercalation rate,  $i_{\text{int}}$  [Eq. (2)]

$$i_{\text{SEI}} = \frac{c^0 D_{\text{Li}} F^2}{2RT \sigma_{\text{Li}^+ \text{SEI}}} e^{-\tilde{\eta}_{\text{SEI}, \text{Li}}} i_{\text{int}} \quad (2)$$

where  $c^0$  is the standard concentration,  $D_{\text{Li}}$  is the diffusion coefficient of Li in the SEI,  $\sigma_{\text{Li}^+ \text{SEI}}$  is the ionic conductivity of  $\text{Li}^+$  across the SEI layer, and  $\tilde{\eta}_{\text{SEI}, \text{Li}}$  is the dimensionless overpotential due to the Li formation. Despite these approaches provide very useful formulas to correlate the SEI growth with experimental observables, 2D approaches are incapable, by

[a] M. Chouchane, Dr. O. Arcelus, Prof. Dr. A. A. Franco  
Laboratoire de Réactivité et Chimie des Solides (LRCS), UMR CNRS 7314  
Université de Picardie Jules Verne  
Hub de l'Energie  
15 rue Baudelocque, 80039 Amiens Cedex, France  
E-mail: alejandro.franco@u-picardie.fr

[b] M. Chouchane, Dr. O. Arcelus, Prof. Dr. A. A. Franco  
Réseau sur le Stockage Electrochimique de l'Energie (RS2E), FR CNRS 3459  
Hub de l'Energie  
15 rue Baudelocque, 80039 Amiens Cedex, France

[c] Prof. Dr. A. A. Franco  
ALISTORE-European Research Institute, FR CNRS 3104  
Hub de l'Energie  
15 rue Baudelocque, 80039 Amiens Cedex, France

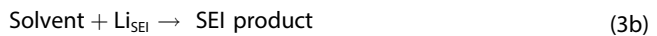
[d] Prof. Dr. A. A. Franco  
Institut Universitaire de France  
103 boulevard Saint Michel, 75005 Paris, France

 Supporting information for this article is available on the WWW under <https://doi.org/10.1002/batt.202100030>

 © 2021 The Authors. *Batteries & Supercaps* published by Wiley-VCH GmbH. This is an open access article under the terms of the Creative Commons Attribution License, which permits use, distribution and reproduction in any medium, provided the original work is properly cited.

construction, to capture the impact of the porous electrode three-dimensional features, such as active material and carbon-binder spatial heterogeneities on the growth process and its impact on the electrode performance. The explicit representation of such mesostructure features is of paramount importance since the SEI formation may initiate at the graphite/electrolyte interface, so an implicit consideration of the carbon and binder domain (CBD) would not capture the actual active surface area loss and the electron transport heterogeneities due to the CBD percolation network.

This communication aims to propose a methodology to investigate the seldom-discussed topic of heterogeneous SEI, for the first time to the authors' knowledge through a 3D-resolved continuum modeling approach with CBD explicitly considered at the mesoscale. For demonstration purposes, we focus here on different half-cells with graphite as the positive electrode's active material (AM) with two different morphologies. The concerned graphite electrodes are 35% porous and were stochastically generated using the software Geodict®. One electrode contains spherical particles (Figure 1a) and the other one contains ellipsoidal particles (Figure 1b). Ellipsoidal particles, despite forming electrodes with high tortuosity factor (Figure 1c), have been identified as a promising morphology through impedance measurements simulations because of their lower resistance due to solid-state diffusion when compared to spherical graphite.<sup>[17]</sup> Then, 8% of volume of CBD was added, using an in-house MATLAB-based algorithm already reported by us.<sup>[18]</sup> A 6 µm thick homogeneous separator was added on top of the graphite electrodes (75 × 75 × 75 µm<sup>3</sup>), the positive electrode's current collector and the Li foil (negative electrode) were considered implicitly. The electrode mesostructures were then imported into the software COMSOL Multiphysics® as meshed volumes using our INNOV algorithm,<sup>[19]</sup> where the classical Newman model<sup>[20–23]</sup> was implemented in three dimensions. Then, an interfacial SEI domain is added only at the graphite/electrolyte interface, the SEI being considered implicitly due to its nanometric thickness. Based on Ref. [16] we assume here that the Li<sup>+</sup> can either be inserted in the graphite or in the SEI where it will later react with the solvent to form SEI as it follows [Eq. (3)]



Similarly to Equation (1), the SEI growth current is assumed in our model to be controlled by

$$i_{\text{SEI}} = k_{\text{SEI}} \sqrt{c_e} \left( e^{\frac{F\eta_{\text{SEI}}}{2RT}} - e^{-\frac{F\eta_{\text{SEI}}}{2RT}} \right) \quad (4)$$

As a consequence, the SEI will grow faster where Li<sup>+</sup> concentration is high and where the overpotential is low. Since the system under study is a half-cell (infinite reservoir of Li at the negative electrode) and the aging is out of the scope of this study, the first discharge will trigger an accelerated SEI formation. Therefore, it is assumed that the SEI layer will not

change during the following charge, so no Li<sup>+</sup> will be consumed for the SEI formation during the charge.

More information regarding the electrode mesostructures generation and the physical model can be found in the Supporting Information.

The simulations consist in a discharge at C/20 vs lithium (equivalent to a charge if the graphite is used as the negative electrode) during which the SEI will be formed and a charge at 1 C. During charge, the SEI thickness is assumed to remain constant and to impact the electrode only as a resistive layer for Li deintercalation. The results of this cycle are then compared to a cycle of the same half-cell but without any SEI contribution. The simulated cycling curves for the spherical and ellipsoidal graphite are reported in Figure 2a. For both spherical and ellipsoidal graphite, the discharges with and without SEI growth are almost identical. As expected, the charge with the SEI displays a higher ohmic loss than the one without SEI for both spherical and ellipsoidal electrodes. However, for the ellipsoidal case, the ohmic loss is much higher than the spherical one, on average 0.147 V vs. 0.033 V respectively when compared with the charge without SEI. This trend would suggest that the impact of the heterogeneous SEI formation differs according to the active material particle morphology. In addition, the electrode with ellipsoidal particles demonstrates a specific capacity much lower than the spherical one (27 vs. 280 mAh.g<sup>-1</sup> respectively for the charge with SEI). Nonetheless, this dramatic difference does not arise from the SEI but rather from a limitation at a high rate of the electrode morphology itself (as detailed later) since poor yield is also observed for the electrode with ellipsoidal particles after the charge without SEI (103 mAh.g<sup>-1</sup>).

To quantify the SEI heterogeneity, the calculated distribution of its thickness within the electrode volume is represented in Figure 2b for both ellipsoidal and spherical graphite at the end of discharge. The variation of values of the SEI thickness is higher for the ellipsoidal electrode (standard deviation  $\sigma_{\text{STD}} = 21.1$  nm) than for the spherical graphite ( $\sigma_{\text{STD}} = 11.6$  nm). It is noteworthy that the average value of SEI thickness is higher for the spheres than for the ellipsoids (45.6 nm and 39.3 nm respectively) because the active surface area is higher for the ellipsoid<sup>[17]</sup> ( $7.79 \times 10^{-8}$  m<sup>2</sup> versus  $7.29 \times 10^{-8}$  m<sup>2</sup> for the spherical) and the time of discharge is lower for the ellipsoid (54629 s versus 63272 s for the spherical). The histogram used for the analysis proves the capability of this modeling approach to form heterogeneous SEI layer dependent on the graphite electrode mesostructure.

To further assess the SEI heterogeneity, the anisotropy of the SEI thickness has been displayed in Figure 2c,d which represents the average value of the SEI thickness within the electrode volume as a function of the distance from the (0,0,0) point (origin of the coordinate system) indicated in Figure 1. While the spherical graphite has a rather isotropic distribution of the SEI thickness (ca. 15 % of variation), the SEI thickness for the ellipsoidal graphite is strongly anisotropic. Indeed, the z-axis trend shows that the SEI near the separator is almost three times thicker than near the current collector, while along the x and y axes variations of the same magnitude as the spherical

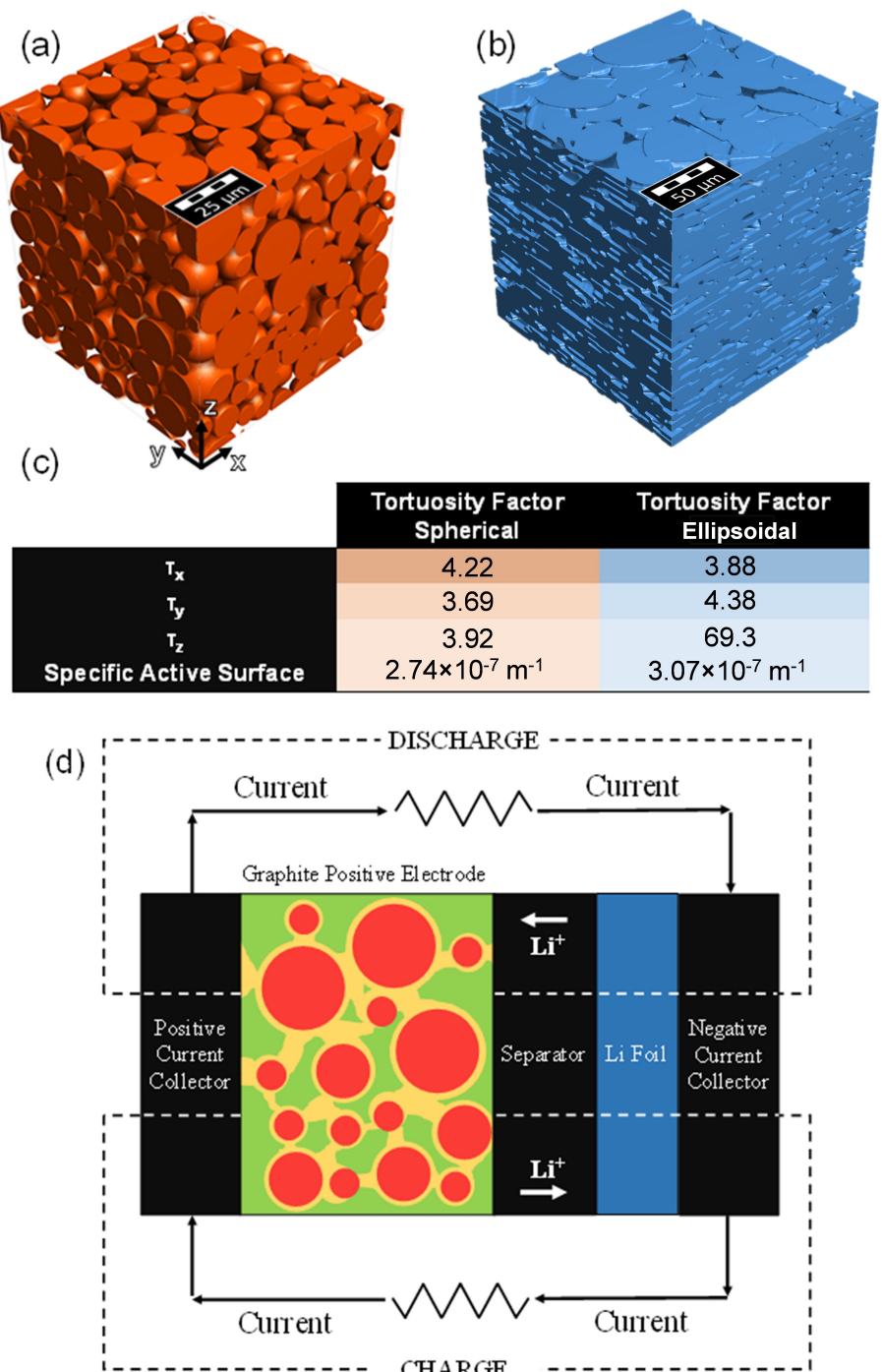


**Figure 1.** 3D rendering of the a) spherical and b) ellipsoidal particles constituting the simulated electrodes, the separator and the current collector are respectively located at the top and the bottom of the electrodes; c) the associated tortuosity factors calculated using TauFactor<sup>[24]</sup> software and the specific active surfaces which are the active surface areas divided by the volumes of graphite. The CBD location can be visualized in the Supporting Information, Figure S2 and in the mesh videos; d) scheme of the simulated system under charge and discharge with the graphite in red, the CBD in orange, and the electrolyte in green.

case are observed. To summarize, in the ellipsoidal case the SEI is the thinnest at the bottom of the electrode and gets thicker as we get closer to the negative electrode side. Such a gradient along the z-direction during discharge in a positive electrode is usually due to ionic transport limitation. Figure S7 (Supporting Information) reports the lithiation state at the end of charge for

both electrodes, and highlights this ionic transport limitation for the ellipsoidal case.

The relative electrolyte concentration profiles at a time of charge equal to 270 s (end of discharge for the ellipsoidal case) for the spherical and ellipsoidal graphite electrodes (with SEI) are respectively represented in Figure 3a,b. In both, the

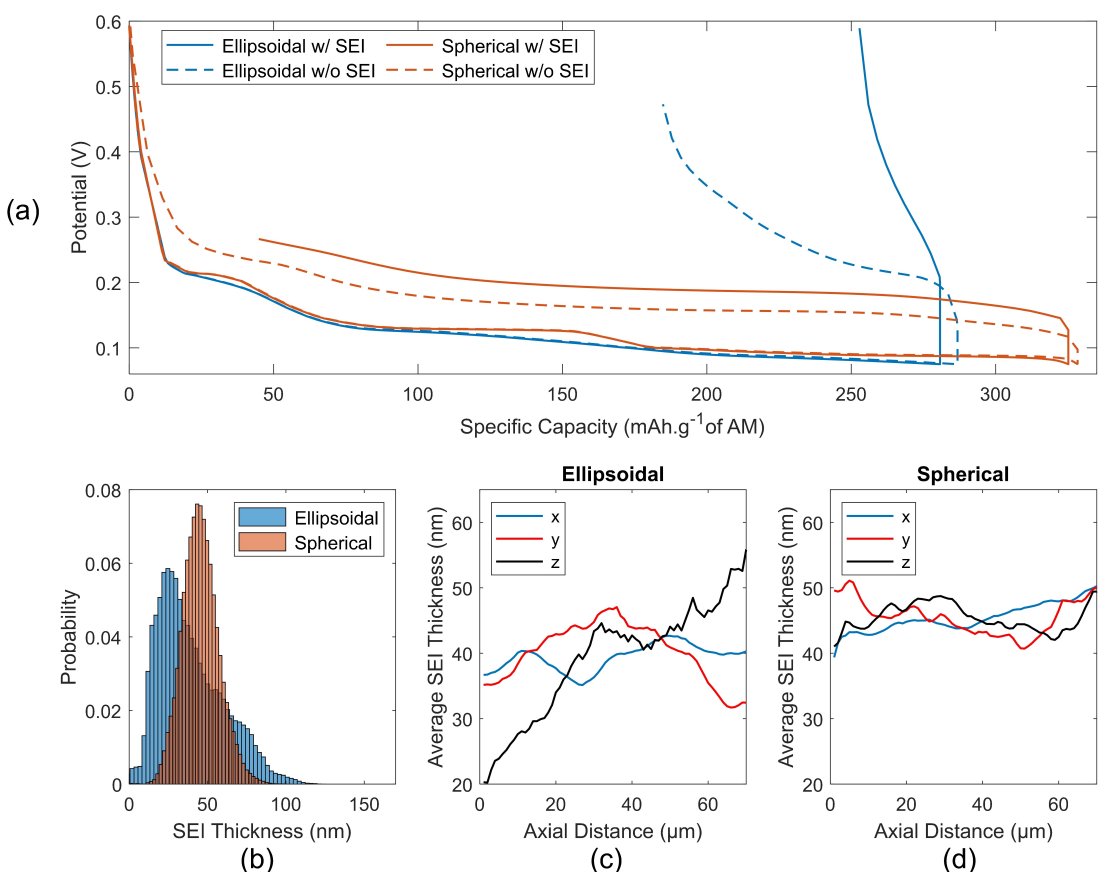


**Figure 2.** a) Simulated cycling curves of both structures with and without SEI. b) The distribution of the SEI thickness at the end of discharge for both cases. The spatial evolution of the SEI thickness along the three axes for c) ellipsoidal and d) spherical graphite.

concentration is higher near the positive electrode's current collector than near the separator side. Indeed, during the charge, Li is deinserted from the positive active material and travels through the electrode and the separator to be deposited into the negative electrode. Since we consider high kinetics for the deposition of Li on the Li foil, the process is limited by the transport of Li<sup>+</sup>, hence this gradient of concentration. Interestingly the gradient is much more pronounced for the ellipsoidal electrode with the electrolyte concentration being almost 10 times higher near the current collector than near the separator. This steep concentration gradient entails the poor specific capacity and the higher ohmic loss during charge reported earlier for the ellipsoidal electrode displayed in Figure 2a. Moreover, it can also explain the anisotropy of the SEI thickness for the ellipsoidal graphite. Indeed, the location of the thicker SEI from Figure 2c stems from the limited ionic transport. During discharge, the Li<sup>+</sup> flows from the negative electrode through the separator to the positive electrode where it intercalates. As it has been evidenced in the ellipsoidal positive electrode, the region near the current collector is poorly connected to the upper part of the electrode. During charge, it leads to an accumulation of ions near the current collector (Figure 3a), but during discharge, it leads to an accumulation of ions near the separator, causing a higher utilization of the upper part of the positive electrode.

This results in a thicker SEI near the separator and a thinner SEI close to the current collector. The calculated anisotropy of the SEI due to the electrode mesostructure further proves the capability of the model to capture the impact of the electrode mesostructure.

Once the discharge and the anisotropy of the SEI have been explained through the structural properties of the electrodes, one should analyze the impact of the heterogeneous SEI layer on the observables along charge. The active surface area has been divided into two sub-surfaces, the half with the thicker SEI ( $S_{\text{thick}}$ ) and the other half with the thinner SEI ( $S_{\text{thin}}$ ) based on the results at the end of the discharge. Figure 3c reports the average difference in lithiation state on both sub-surfaces at different times along charge (with and without SEI) for the two electrode mesostructures. In the spherical graphite electrode, a higher difference is observed for the charge with SEI than for the charge without SEI. This effect is due to the SEI preventing the Li to be deinserted where the layer is the thickest due to a higher overpotential. Moreover, the difference in the average lithiation state reaches a peak around 1500 s of charge and then decreases until the end of charge. This evolution can be explained by the average rates at which the active material delithiate at  $S_{\text{thick}}$  and  $S_{\text{thin}}$  (Figure 3d). During the first half of the charge, the deinsertion of Li is favored at  $S_{\text{thin}}$  where the SEI is the thinnest with an average rate value of

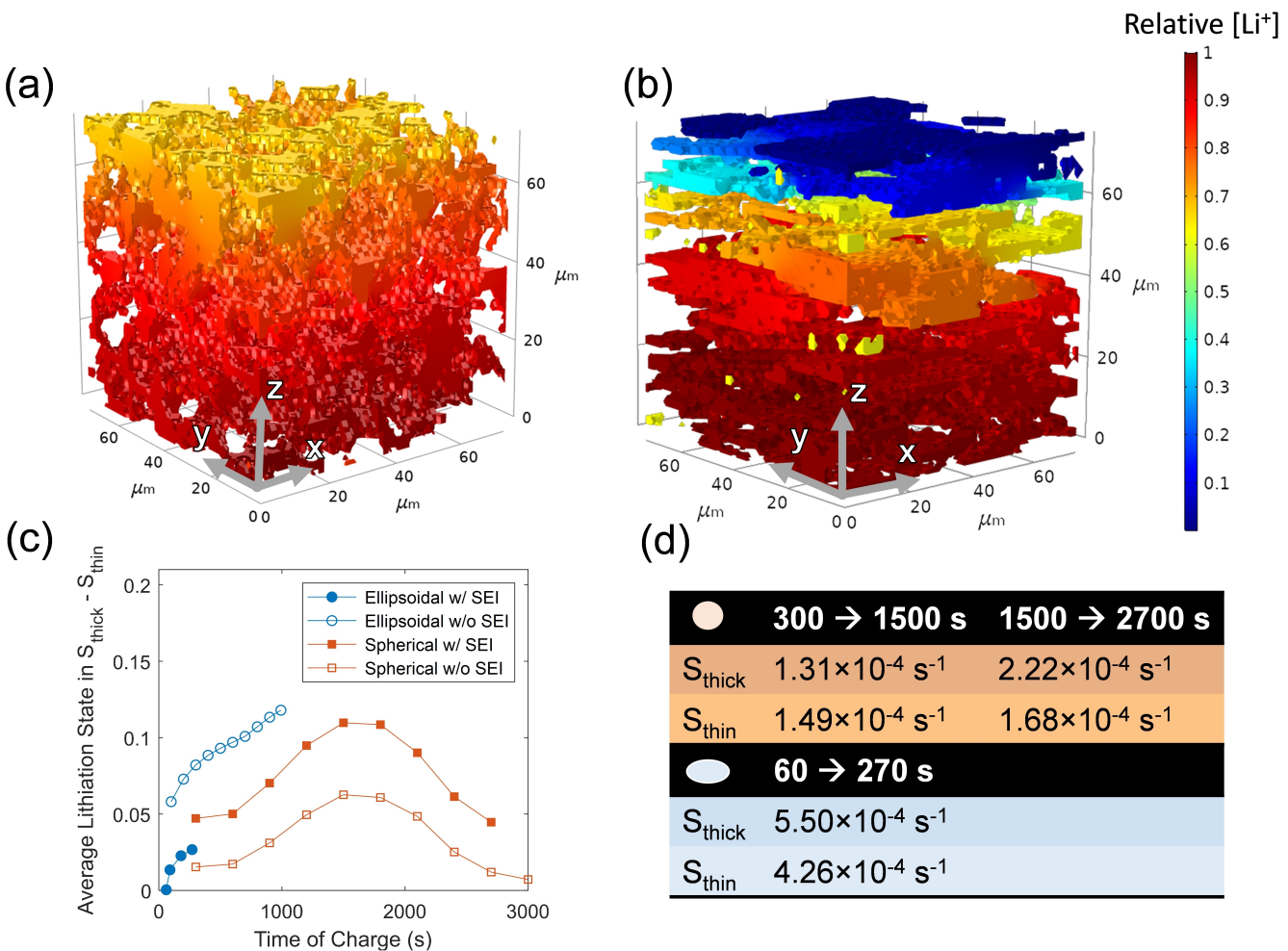


**Figure 3.** 3D representation of the relative electrolyte concentration ( $[\text{Li}^+]/[\text{Li}^+]_{\text{max}}$ ) at time = 270 s for the charge simulation with SEI for a) the spherical particles; b) the ellipsoidal particles as calculated by our electrochemical model, the separator and the current collector are located at the top and at the bottom of the electrodes, respectively; c) evolution of the difference of the average lithiation state between the surface  $S_{\text{thick}}$  (half of the active surface where the SEI is thicker) and  $S_{\text{thin}}$  (half of the active surface where the SEI is thinner) during the charge simulation with SEI; d) the average rate of delithiation at  $S_{\text{thick}}$  and  $S_{\text{thin}}$  along time during the charge simulation with SEI for the spherical particles (in orange) and the ellipsoidal ones (in blue).

$1.49 \times 10^{-4} \text{ s}^{-1}$  versus  $1.31 \times 10^{-4} \text{ s}^{-1}$  for  $S_{\text{thick}}$ , leading to an increase of the heterogeneity. However, once the lithiation state at  $S_{\text{thin}}$  reaches a threshold, it becomes more favorable for the lithium to be deinserted at  $S_{\text{thick}}$  where the lithium content is the highest, even though the SEI is the thickest. Indeed, the rate of delithiation increases by 60% after 1500 s at  $S_{\text{thick}}$  while only by 10% at  $S_{\text{thin}}$ , hence a homogenization of the system and a decrease of the difference in average lithiation between the two sub-surfaces is observed. Regarding the electrode with ellipsoidal particles, the same increase of the difference in average lithiation is reported but since the charge could not last long because of the ionic transport limitation, the following decrease could not be observed. It is noteworthy that the trend is reversed for the ellipsoidal compared to the spherical case, indeed the charge without SEI has a higher heterogeneity in terms of lithiation than the one with SEI. As seen previously, part of the electrode with ellipsoidal particles will be highly favored for the deinsertion because of a poorly connected electrolyte phase. So during the charge, the lithium will not have as much freedom as in the spherical graphite to be

deintercalated where the SEI is the thinnest: it will mainly be constrained to react in the upper part of the electrode, near the separator. It entails a higher deintercalation rates at  $S_{\text{thick}}$  ( $5.50 \times 10^{-4} \text{ s}^{-1}$ ) than at  $S_{\text{thin}}$  ( $4.26 \times 10^{-4} \text{ s}^{-1}$ ) for the charge with SEI, which is also a cause of the high ohmic loss reported previously. Since the SEI layer is the thickest in the upper part of the electrode, the SEI will still favor a deinsertion at the bottom of the electrode, where it was the least favorable in the case of the charge without SEI. It will tend to reduce the heterogeneity in the system, hence the observed trend between the two ellipsoidal case curves in Figure 3c. However, this homogenization of the system is not beneficial to the overall performance of the electrode, since it occurs at the prize of a significant ohmic loss, and the poor utilization of the cell remains due to a poorly connected electrolyte phase.

The impact of the heterogeneous SEI is clearly visible in Figure 4 which reports 3-D slice views of both electrodes at the time of charge at which the difference between  $S_{\text{thick}}$  and  $S_{\text{thin}}$  is the highest (i.e. 270 s for ellipsoidal and 1500 s for spherical graphite particles). For the electrode with spherical particles,

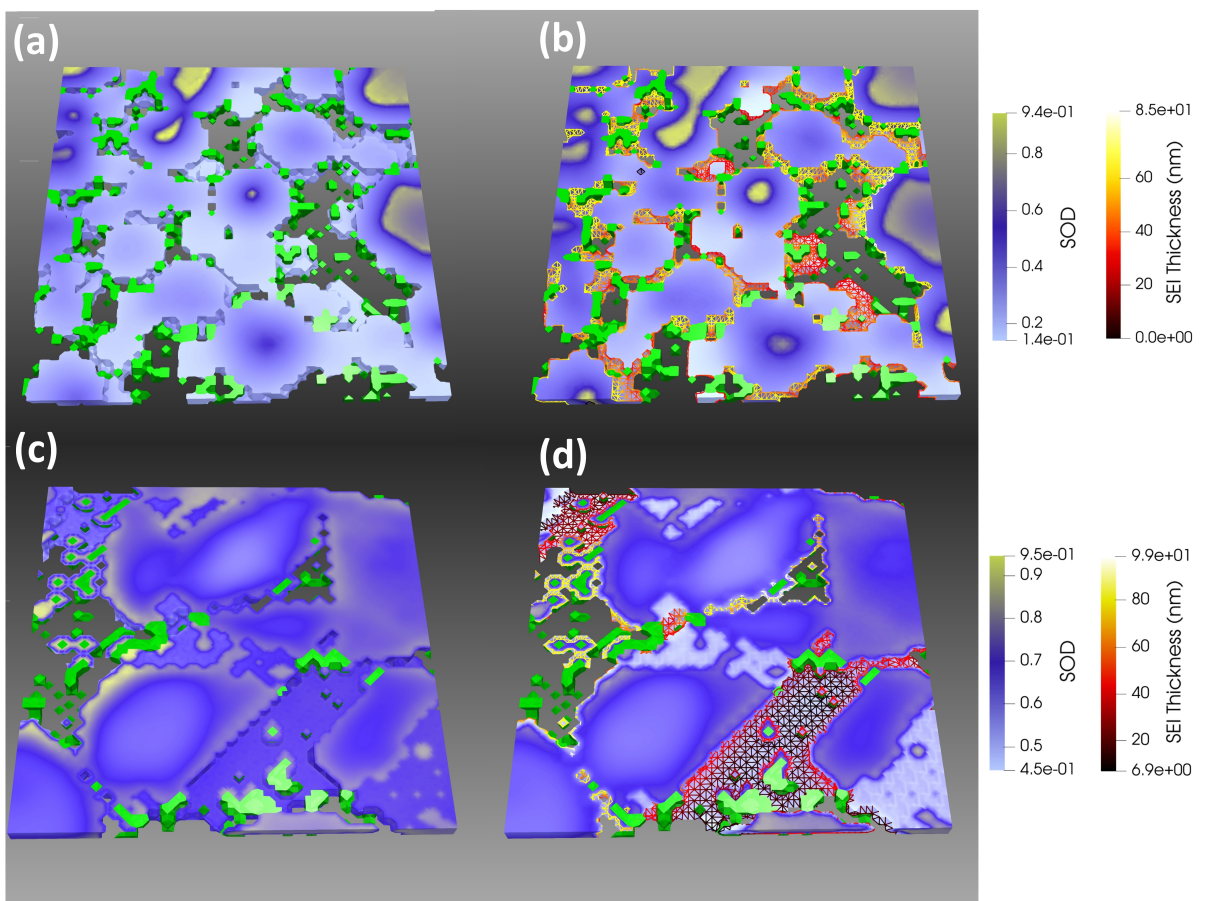


**Figure 4.** 3D representations of the relative State of Discharge (SOD) for a time of charge = 1500 s and  $67 \mu\text{m} < z < 70 \mu\text{m}$  for the electrode with spherical particles a) without and b) with SEI, and for a time of charge = 270 s and  $37 \mu\text{m} < z < 40 \mu\text{m}$  for the electrode with ellipsoidal particles c) without and d) with SEI. The CBD is represented in green, the SEI thickness as wireframe in thermal scale. The separator and the current collector are respectively located at the top and the bottom of the electrode slices.

the state of discharge (SOD) is more homogeneous without SEI (Figure 4a) than with SEI (Figure 4b). The Li concentration is higher where the SEI is the thickest (yellow wireframe) and lower where the SEI is the thinnest (dark red wireframe). Hence a deinsertion of Li favored where the SEI is the thinnest leading to higher heterogeneities. The opposite trend is observed for the electrode with ellipsoidal particles where the distribution of SOD is more heterogeneous during the charge without SEI (Figure 4c) than with SEI (Figure 4d). As explained earlier, this is due to the SEI being thinner where it is the least favorable for the Li to be deinserted in the case without SEI. For instance, in Figure 4(c,d), in this slice near the bottom half of the electrode with ellipsoidal particles ( $37 \mu\text{m} < z < 40 \mu\text{m}$ ), the average SOD is lower in the case with SEI than compared to the case without SEI. It was shown that due to ionic limitation, this region of the electrode with ellipsoidal particles was poorly utilized. During the charge with SEI, it will then be more favorable (thanks to the thinner SEI) for the Li to be deinserted in this region where it was the least favorable before, entailing a homogenization of the SOD. Indeed, the model highlights the influence of the electrode's mesostructure in the SEI formation process, and its impact on the electrochemical performance. In both cases, it results in an ohmic loss but the SEI will have a higher influence

on the ellipsoidal graphite since the system does not have the time to equilibrate along the charge because  $S_{\text{thick}}$  never becomes more favorable for the deintercalation of lithium.

To conclude, this work presents a novel 4D-resolved computational approach to assess heterogeneous SEI growth impact on graphite porous electrode performance. However, there is still room for improvement for the description of the SEI formation step in the model, for instance by introducing several formation cycles. Nevertheless, the model has proven to be capable to form heterogeneous SEI layers and predict their spatial distribution as function of the graphite type (spherical or ellipsoidal particles). It was found that the thickness of the SEI becomes more homogeneous in the spherical electrode where the ionic transport limitation is the mildest, which leads to a better electrochemical performance. We believe that this work provides an insightful tool to assist experimental SEI analysis and, we hope, to stimulate future advanced characterizations of this complex and fascinating interphase.

## Acknowledgements

The authors acknowledge Simon Malifarge (LRCS, Amiens) for the experimental data of the open-circuit voltage and diffusion coefficient of Li inside the graphite as a function of the lithiation state, as well as for the information about the morphology of the ellipsoidal particles. M.C. and A.A.F. acknowledge the European Union's Horizon 2020 research and innovation program for the funding support through the European Research Council (grant agreement 772873, "ARTISTIC" project). O.A. and A.A.F. acknowledge the Région Hauts de France for funding support. A.A.F. acknowledges the Institut Universitaire de France for the support. The authors acknowledge the MatriCS computing cluster and Jean-Baptiste Hoock at the Université de Picardie Jules Verne for technical support.

## Conflict of Interest

The authors declare no conflict of interest.

**Keywords:** lithium-ion battery negative electrode · solid-electrolyte interphase · electrode mesostructure · carbon binder domain · 4D computational modeling

- [6] R. Fong, U. von Sacken, J. R. Dahn, *J. Electrochem. Soc.* **1990**, *137*, 2009–2013.
- [7] D. Guyomard, J. M. Tarascon, *J. Electrochem. Soc.* **1993**, *140*, 3071–3081.
- [8] E. Peled, S. Menkin, *J. Electrochem. Soc.* **2017**, *164*, A1703–A1719.
- [9] D. Li, D. Danilov, Z. Zhang, H. Chen, Y. Yang, P. H. L. Notten, *J. Electrochem. Soc.* **2015**, *162*, A858–A869.
- [10] X. Lin, J. Park, L. Liu, Y. Lee, A. M. Sastry, W. Lu, *J. Electrochem. Soc.* **2013**, *160*, A1701–A1710.
- [11] M. T. Lawder, P. W. C. Northrop, V. R. Subramanian, *J. Electrochem. Soc.* **2014**, *161*, A2099–A2108.
- [12] A. A. Tahmasbi, T. Kadyk, M. H. Eikerling, *J. Electrochem. Soc.* **2017**, *164*, A1307–A1313.
- [13] F. Röder, V. Laue, U. Krewer, *Batteries Supercaps.* **2019**, *2*, 248–265.
- [14] S. Hein, A. Latz, *Electrochim. Acta* **2016**, *201*, 354–365.
- [15] M. B. Pinson, M. Z. Bazant, *J. Electrochem. Soc.* **2013**, *160*, A243–A250.
- [16] L. Kolzenberg, A. Latz, B. Horstmann, *ChemSusChem* **2020**, *13*, 3901–3910.
- [17] B. T. Habte, F. Jiang, *Solid State Ionics* **2018**, *314*, 81–91.
- [18] M. Duquesnoy, T. Lombardo, M. Chouchane, E. N. Primo, A. A. Franco, *J. Power Sources* **2020**, *480*, 229103.
- [19] M. Chouchane, A. Rucci, A. A. Franco, *ACS Omega* **2019**, *4*, 11141–11144.
- [20] M. Chouchane, E. N. Primo, A. A. Franco, *J. Phys. Chem. Lett.* **2020**, *11*, 2775–2780.
- [21] M. Chouchane, A. Rucci, T. Lombardo, A. C. Ngandjong, A. A. Franco, *J. Power Sources* **2019**, *444*, 227285.
- [22] X. Lu, S. R. Daemi, A. Bertei, M. D. R. Kok, K. B. O'Regan, L. Rasha, J. Park, G. Hinds, E. Kendrick, D. J. L. Brett, P. R. Shearing, *Joule* **2020**, *4*, 1–23.
- [23] X. Lu, S. A. Bertei, D. P. Finegan, C. Tan, R. Daemi, J. S. Weaving, K. B. O'Regan, T. M. M. Heenan, G. Hinds, E. Kendrick, D. J. L. Brett, P. R. Shearing, *Nat. Commun.* **2020**, *11*, 1–13.
- [24] S. J. Cooper, A. Bertei, P. R. Shearing, J. A. Kilner, N. P. Brandon, *SoftwareX* **2016**, *5*, 203–210.

Manuscript received: February 1, 2021

Revised manuscript received: April 14, 2021

Accepted manuscript online: April 15, 2021

Version of record online: May 7, 2021